Simulation of Magnetized Target Fusion Experiments at General Fusion

Aaron Froese[1], Meritt Reynolds[1], Sandra Barsky[1], Peter de Vietien[1], Gabór Tóth[2], Dylan Brennan[3], Bick Hooper[4]

[1] General Fusion Inc., Burnaby, British Columbia, Canada
[2] CSEM, University of Michigan, Ann Arbor, Michigan, USA
[3] PPPL, Princeton University, Princeton, New Jersey, USA
[4] Lawrence Livermore National Laboratory (retired), Livermore, CA, USA

APS DPP Conference San Jose, California Oct. 31- Nov. 5, 2016 **CP10.00108**

INTRODUCTION

General Fusion aims to develop a magnetized target fusion (MTF) power plant based on compression of magnetically-confined plasma by liquid metal. General Fusion is testing this compression concept by collapsing solid aluminum liners onto spheromak and tokamak plasmas. The experimental program is supported by various numerical models, including hydrodynamic simulations (both standard and magnetic), equilibrium solvers, and stability analysis codes. Using these tools, we have designed a more favorable compression in spherical tokamak geometry, realized in the positive D-shape of the SPECTOR machine.

SIMULATION CODES IN ACTIVE USE

VAC (Versatile Advection Code) [1]
- Native Features:
  - Conservative shock-capturing finite volume code
  - Single-fluid MHD equations
  - 2D/3D general coordinates
- General Fusion Additions:
  - Coupling to external circuits
  - Compression by moving metal walls
  - Independent electron and ion temperatures
  - Novel algorithm for anisotropic thermal conduction
- Primary Usage:
  - Compact toroid formation and acceleration
  - MHD simulation in static geometry
  - MHD simulation of dynamic compression of plasma

NIMROD [2]
- Native Features:
  - Spectral finite-element discretization in poloidal 2D plane
  - Finite Fourier series in toroidal direction
  - Semi-implicit and implicit temporal discretization
  - Two-fluid effects, kinetic effects, and Hall term
- General Fusion Additions:
  - Poloidal flux boundary conditions in NIMEQ
  - Compression by moving metal walls (in progress)
- Primary Usage:
  - Compact toroid formation
  - MHD simulation in static geometry
  - Linear stability analysis

Caltrans/Corsica [3]
- Native Features:
  - Solves 2D Grad-Shafranov equation
  - Fits profile parameters to experimental data
- General Fusion Additions:
  - Better support for multiple geometries
  - Ability to import vacuum fields from FEMM
- Primary Usage:
  - Fitting magnetic probe data to GS model

DCON / Resistive DCON [4]
- Native Features:
  - Calculates ideal and resistive MHD stability
  - Uses very efficient Newcomb algorithm
  - Static axisymmetric toroidal geometries
- Primary Usage:
  - Linear MHD stability analysis during compression

FEMM (Finite Element Method Magnetics)
- Native Features:
  - Solves low-frequency electromagnetic problems in 2D
  - Supports nonlinear magnetic materials
- Primary Usage:
  - Modelling gun flux in plasma injectors

LS-DYNA
- Native Features:
  - Finite element analysis with explicit time integration
  - Includes nonlinear material physics
  - Includes multiphysics and fluid-structure interactions
- Primary Usage:
  - Modelling implosion of solid aluminum flux conserver

MACHINE DESIGN

PROSPECTOR was designed to create a tokamak configuration in a geometry that was compatible with a cylindrical pinch implosion. A toroidal flux dump was included so that the toroidal magnetic field in the flux conserver could be easily pushed away during formation.

SPECTOR 1 was designed to have a positive D-shape, which is known (and was calculated) to improve plasma stability. The toroidal flux dump was found to be unnecessary, so the diagnostic head plate was simplified. The DC magnetic circuits were placed so that most of the gun flux crossed the electrodes above the formation electrode.

SPECTOR 2B has a modified shaft in the flux conserver to more closely match the trajectory of the flux conserver during a bottom-up implosion.

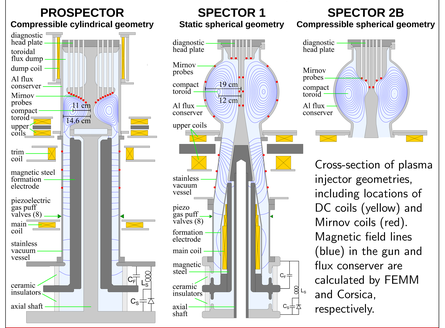

Cross-section of plasma injector geometries, including locations of DC coils (yellow) and Mirnov coils (red). Magnetic field lines (blue) in the gun and flux conserver are calculated by FEMM and Corsica, respectively.

PLASMA STABILITY

We evaluate the sensitivity of the plasma stability to changes in geometry, shaft current, β, and current density (λ) profile (parametrized by slope α). Stability maps show the linear growth rates for such a set of NIMROD simulations. Stable conditions are shown in cyan. Unstable conditions are coloured by the growth rate of the most unstable mode and numbered by its toroidal mode number n.

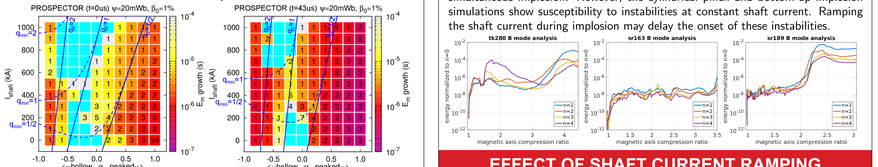

The above plots show the stability regions for uncompressed (left) and partially compressed (right) PROSPECTOR geometries at $\beta = 1\%$ and resistivity equivalent to $T_e = 10$ eV. The range of parameters that permit a stable CT becomes smaller as the compression proceeds.

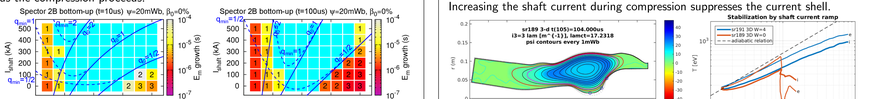

In comparison, the uncompressed (left) and partially compressed (right) SPECTOR 2B geometries exhibit much better stability.

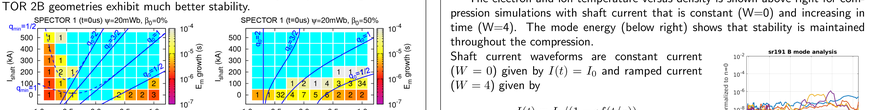

Pressure effects are shown in an uncompressed SPECTOR 1 geometry for β on axis of 0% and 50% (peaked profile). Beta stabilizes hollow λ profiles, but allows an internal kink to develop if $q_0 < 1$.

MHD COMPRESSION SIMULATIONS

Results from LS-Dyna are used to define the mesh shape for VAC simulations. The results from both simulations are superimposed below. Chemical accelerants and their exhaust gases are pale yellow, while the aluminum flux conserver is gray. The normalized current density $\lambda \equiv \mu_0 \mathbf{J} \cdot \mathbf{B}/\mathbf{B} \cdot \mathbf{B}$ is shown on a green-blue scale, while the $\psi/\psi_{max} = 95\%$ and 86% surfaces appear in magneta and red.

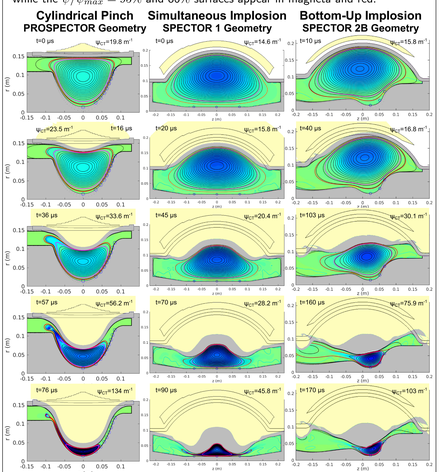

For each compression geometry above, the energy in each mode is plotted below. Simulations demonstrate that the CT remains MHD stable throughout the simultaneous implosion. However, the cylindrical pinch and bottom-up implosion simulations show susceptibility to instabilities at constant shaft current. Ramping the shaft current during implosion may delay the onset of these instabilities.

EFFECT OF SHAFT CURRENT RAMPING

In the simulations shown above, numerical dissipation prevents the formation of a current shell. In low dissipation simulations, a shell (below left) develops at constant shaft current because the plasma attempts to preserve its internal q profile. Increasing the shaft current during compression suppresses the current shell.

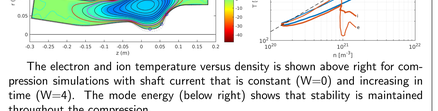

The electron and ion temperature versus density is shown above right for compression simulations with shaft current that is constant (W=0) and increasing in time (W=4). The mode energy (below right) shows that stability is maintained throughout the compression.

Shaft current waveforms are constant current ($W = 0$) given by $I(t) = I_0$ and ramped current ($W = 4$) given by

$$I(t) = I_0/(1 - cf(t/\tau))$$

$$f(x) = (1 + x^a)^{1/a} - 1$$

with $c = 0.227$, $t_0 = 40\mu$s, and $a = 6$.

COMPARISON OF SIMULATION AND EXPERIMENT

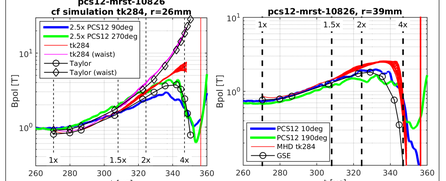

In the PCS12 experiment (PROSPECTOR geometry) the poloidal magnetic probe signals are a combination of intrinsic evolution of the CT and its "pulling away" from the probes as it is compressed toward the shaft. The data on deep compression comes from the innermost probes. These read lower values than the 3D MHD simulation after 2x compression. The curve label "GSE" indicates the geometry-dependent solution of the Grad-Shafranov eigenvalue equation $\Delta^* \psi = \lambda_{\rm GE}^2 \psi$. It is not a Taylor-relaxed state, but has the same $\psi(r, z)$ and flux-conserver eigenvalue $\lambda_{\rm GE}$. The GSE curves assume constant poloidal flux, and represent the inner probe signals surprisingly well.

In the PCS13 experiment (spherical tokamak geometry), mode activity manifests about $34\,\mu$s after compression begins, in contrast to an MHD prediction of $130\,\mu$s due to formation and disruption of the current shell. The initial amplification of poloidal field in the experiment, prior to significant mode activity, is more consistent with a hollow current profile than a peaked one. Conjecture: The compression target already had a current shell that was soon destabilized by compression.

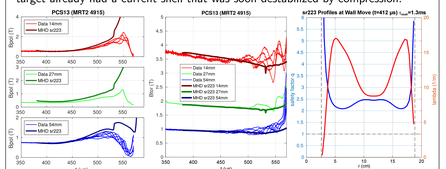

The left and middle figures compare poloidal and toroidal magnetic fields measured by the surface probes in PCS13 with an MHD simulation (sr223). Simple initial current density profiles overestimate poloidal field growth during compression. In this case, the shaft current in a static geometry was allowed to decay for 30 μs with a time constant of $\tau_{\rm shaft} = 1.3$ ms. This created the λ and q profiles in the right figure. This shell current profile was able to reproduce the magnetic field amplification observed until late in the compression (120 μs after wall move).

In the PROSPECTOR geometry, unfavorable curvature results in low calculated beta limits. However, simulation shows near-adiabatic compression until low-n current-driven modes destroy flux surfaces.

COMPARISON OF PLASMA STABILITY CODES

To understand the effect of resistivity, we compare the stability predicted by DCON (ideal MHD) with that predicted by NIMROD (resistive MHD). The stability of a CT with a peaked lambda profile in the SPECTOR 1 bottom-up implosion geometry is below. The flux conserver becomes flatter towards 100 μs, causing the n=1 mode to become unstable for cases with low q (low shaft current).

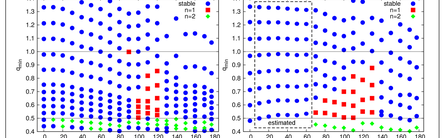

Resistivity has a destabilizing effect, allowing the CT to become n=1 unstable earlier in the compression, but only at lower values of q. Stability to n=1 returns after 130 μs because the flux conserver has pinched off the gun and the equilibrium is contained within a smaller volume with low elongation.

This result shows clearly that stability can be retained by ensuring a sufficiently high minimum q. This is accomplished by ramping the shaft current during the compression.

EXTERNAL MODE STABILITY

The stability of SPECTOR 1 to external modes was evaluated in uncompressed ($R/R_0 = 1.0, t = 0\,\mu$s) and compressed ($R/R_0 = 0.27, t = 90\,\mu$s) geometries using DCON. A map of cases with a peaked λ profile ($\alpha = 0.53$) and $\beta_0 \sim 7\%$ was made by scaling the shaft and plasma current. The red dot on each plot indicates a case where the plasma and shaft currents scale inversely with the compression. Coloured contours indicate stable regions and blank regions are unstable. As the CT is compressed, the number and area of the unstable regions grow.

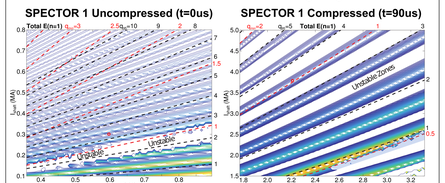

A VAC MHD simulation of a SPECTOR 1 simultaneous implosion predicts stability even when $q_0 < 1$. The stability of this plasma was analyzed with Resistive DCON for the late compression period. Ideal MHD analysis with DCON shows positive energy for both $n = 1$ and $n = 2$ confirming the VAC prediction of stability (below left). Energy oscillations occur as resonant q values pass through the edge of the plasma during compression.

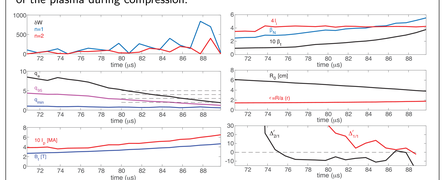

Resistive DCON shows that the tearing mode drive Δ' is generally negative (stable) for the $2/1$ mode but positive (unstable) for the $1/1$ mode (above right). This instability did not manifest in the VAC simulation, perhaps being stabilized by pressure or viscosity.

EFFECT OF SAFETY FACTOR PROFILE q(ψ)

Spheromak and tokamak configurations have nearly the same geometry and vary only by the shaft current. The tokamak has a monotonic q profile, but the spheromak has a minimum in q. We use DCON to compare the free-boundary, ideal MHD stability of these two cases.

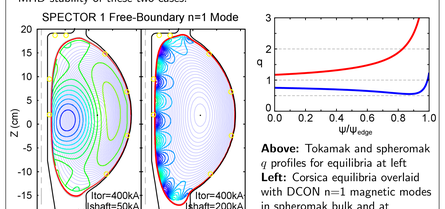

Above: Tokamak and spheromak q profiles for equilibria at left
Left: Corsica equilibria overlaid with DCON n=1 magnetic modes in spheromak bulk and at tokamak edge

DCON is built into Corsica [4,5]. It checks stability criteria for inverse equilibria, in this case showing that the tokamak configuration is more stable than the spheromak case.

Internal Stability Criteria

Mercier	Unstable at minimum q	stable
Ballooning	stable	stable
Resistive Modes	Unstable near magnetic axis	Unstable near magnetic axis

- Both geometries are sensitive to external currents and magnetic fields.
- The gun current may need to be adjusted during compression.
- The spheromak n=1 free-boundary mode couples to a mode at minimum q.
- The spheromak is more sensitive to variations in the external currents.

MHD EQUATIONS IN VAC

MHD equations are solved using the finite-volume code VAC. We evolve the mass density ρ, momentum density $\rho\mathbf{v}$, magnetic induction $\mathbf{B}$, electron thermal energy density $e_{\rm th,e}$, ion thermal energy density $e_{\rm th,i}$, electron parallel heat flux $q_{\parallel,\rm e}$, and ion parallel heat flux $q_{\parallel,\rm i}$.

$$\frac{\partial \rho}{\partial t} + \nabla \cdot (\mathbf{v}\rho) = 0$$

$$\frac{\partial (\rho \mathbf{v})}{\partial t} + \nabla \cdot (\mathbf{v}\rho\mathbf{v} - \mu_0^{-1}\mathbf{B}\mathbf{B}) + \nabla p_* = \nabla \cdot \boldsymbol{\Upsilon}$$

$$\frac{\partial \mathbf{B}}{\partial t} + \nabla \cdot (\mathbf{v}\mathbf{B} - \mathbf{B}\mathbf{v}) = -\nabla \times \mathbf{E}'$$

$$\frac{\partial e_{\rm th,e}}{\partial t} + \nabla \cdot (\mathbf{v} e_{\rm th,e}) = -(\gamma - 1) e_{\rm th,e} \nabla \cdot \mathbf{v} + G_{\rm ei} - \nabla \cdot \mathbf{q}_{\rm e} + \mathbf{E}' \cdot \mathbf{J}$$

$$\frac{\partial e_{\rm th,i}}{\partial t} + \nabla \cdot (\mathbf{v} e_{\rm th,i}) = -(\gamma - 1) e_{\rm th,i} \nabla \cdot \mathbf{v} - G_{\rm ei} - \nabla \cdot \mathbf{q}_{\rm i} + \boldsymbol{\Lambda} : \boldsymbol{\Upsilon}$$

$$\frac{\partial q_{\parallel,\rm e}}{\partial t} + \nabla \cdot (\mathbf{v} q_{\parallel,\rm e}) = -\frac{5}{2} n_{\rm e} \frac{kT_{\rm e}}{m_{\rm e}} \frac{\mathbf{B}}{|\mathbf{B}|} \cdot \nabla (kT_{\rm e}) - \frac{q_{\parallel,\rm e}}{\tau_{q,\rm e}}$$

$$\frac{\partial q_{\parallel,\rm i}}{\partial t} + \nabla \cdot (\mathbf{v} q_{\parallel,\rm i}) = -\frac{5}{2} n_{\rm i} \frac{kT_{\rm i}}{m_{\rm i}} \frac{\mathbf{B}}{|\mathbf{B}|} \cdot \nabla (kT_{\rm i}) - \frac{q_{\parallel,\rm i}}{\tau_{q,\rm i}}$$

Thermal pressure p and total pressure p_* are given by

$$p = (\gamma - 1)(e_{\rm th,e} + e_{\rm th,i}) \qquad p_* = p + \mu_0^{-1} B^2/2$$

with $\gamma = 5/3$. The current density is given by $\mathbf{J} = \mu_0^{-1} \nabla \times \mathbf{B}$. The Ohm's law electric field $\mathbf{E}'$ is taken to be purely resistive with an isotropic resistivity η:

$$\mathbf{E}' = \mathbf{E} + \mathbf{v} \times \mathbf{B} = \eta \mathbf{J}$$

Temperature-dependent Spitzer resistivity $\eta(T_{\rm e}) \simeq (4.6 \times 10^{-4}\,\Omega\,{\rm m})(1\,{\rm eV}/T_{\rm e})^{3/2}$.

By treating $q_{\parallel,\rm e}$ and $q_{\parallel,\rm i}$ as dynamical quantities we avoid the diffusive time step limit. The heat fluxes are given by

$$\mathbf{q}_{\rm e} = \frac{\mathbf{B}}{|\mathbf{B}|} q_{\parallel,\rm e} - \kappa_{\perp,\rm e} \nabla (kT_{\rm e}) \qquad \mathbf{q}_{\rm i} = \frac{\mathbf{B}}{|\mathbf{B}|} q_{\parallel,\rm i} - \kappa_{\perp,\rm i} \nabla (kT_{\rm i})$$

with Braginskii expressions for $\kappa_{\perp,\rm e}$ and $\kappa_{\perp,\rm i}$ (also $\tau_{q,\rm e}$ and $\tau_{q,\rm i}$). The decomposition into parallel and isotropic is equivalent to parallel and perpendicular when $\kappa_\parallel \gg \kappa_\perp$ but easier to implement. Use constant isotropic viscosity $\mu = 6 \times 10^{-6}\,{\rm kg\,m^{-1}\,s^{-1}}$. Viscous stress tensor $\boldsymbol{\Upsilon} = 2\mu\boldsymbol{\Lambda}$ with $2\boldsymbol{\Lambda} = (\nabla \mathbf{v}) + (\nabla \mathbf{v})^{\rm T} - \frac{1}{3}{\rm Tr}\left[(\nabla \mathbf{v}) + (\nabla \mathbf{v})^{\rm T}\right]$

IMPLEMENTATION OF MOVING MESH IN VAC

Compression by moving wall is done using a quasi-static method ($v_{\rm liner} \ll v_{\rm Alfvén}, v_{\rm sound}$). First we transform physical quantities to invariant ones:

$e_{{\rm th},s}^{3/2}/\rho^{5/2} \quad s = {\rm e,i}$	Specific entropy measure
$\sqrt{g}\rho$	Mass tensor density
$\sqrt{g}\rho v_i \quad i = 1,2,3$	Momentum tensor density
$\sqrt{g}B^i \quad i = 1,2,3$	Magnetic flux tensor density

(Tensor components and $\sqrt{g}$ are with respect to logical coordinates. By using covariant momentum we conserve angular momentum. By using contravariant magnetic field we conserve flux.) Then we update the geometry according to LS-DYNA simulation. Finally we transform invariants back to physical quantities.

Typical initial conditions are $I_{\rm shaft} = 300\,{\rm kA}$, $I_{\rm plas} = 250\,{\rm kA}$, $\psi = 15\,{\rm mWb}$, $n = 10^{20}\,{\rm m^{-3}}$ ($\rho = 3.34 \times 10^{-7}\,{\rm kg\,m^{-3}}$ for deuterium plasma), $T_{\rm e} = T_{\rm i} = 200\,{\rm eV}$.

Boundary conditions are zero velocity relative to moving wall, zero temperature (with diffusivities limited to $100\,{\rm m^2/s}$), flux conserving liner ($\mathbf{B} \cdot \mathbf{n} = 0$, $\mathbf{E} \times \mathbf{n} = 0$).

Grid $(n_r, n_z, n_\varphi) = (50, 346, 32)$ refining to $n_z = 582$ during compression.

MHD evolutions uses predictor-corrector TVDLF with Woodward limiter using projection and 8-wave method to suppress monopoles. Alfvén speed and electron sound speed impose similar time step limits in these simulations.

The simultaneous implosion simulation shows robustly stable compression to approximately 4:1 linear compression (density increased by factor 60), at which time there is metal-to-metal contact. This stability persists in VAC simulations with low numerical reconnection (reducing the Rusanov flux in the induction equation). In this case, a current shell forms but is stabilized by the favorable flux conserver shape.

REFERENCES

[1] G. Tóth, Astrophys Lett Commun 34:245 (1996) pp 471.
[2] C.R. Sovinec et al., J. Comp. Phys. 195 (2004) pp 355.
[3] J.A. Crotinger, et al., LLNL Report UCRL-ID-126284 (1997).
[4] A.H. Glasser, J.M. Greene, and J.L. Johnson, Phys. Fluids 18 (1975) pp 875.
[5] E.B. Hooper, et al., Nucl. Fusion 39:7 (1999) pp 693.